Published online 5 April 2017

Nucleic Acids Research, 2017, Vol. 45, No. 11 ***6375–6387***
doi: 10.1093/nar/gkx224

Molecular basis for the methylation specificity of ATXR5 for histone H3

Elisa Bergamin[1], Sabina Sarvan[1], Josée Malette[1], Mohammad S. Eram[2], Sylvain Yeung[1], Vanessa Mongeon[1], Monika Joshi[1], Joseph S. Brunzelle[3], Scott D. Michaels[4], Alexandre Blais[1], Masoud Vedadi[2,5] and Jean-François Couture[1,*]

[1]Ottawa Institute of Systems Biology, Department of Biochemistry, Microbiology and Immunology, University of Ottawa, 451 Smyth Road, Ottawa, Ontario K1H 8M5, Canada, [2]Structural Genomics Consortium, University of Toronto, Toronto, Ontario M5J 1L7, Canada, [3]Northwestern Synchrotron Research Center, Life Sciences Collaborative Access Team, Northwestern University, Argonne, IL 60439, USA, [4]Department of Biology, Indiana University, 915 East Third Street, Bloomington, IN 47405, USA and [5]Department of Pharmacology and Toxicology, University of Toronto, 1 King's College Circle, Toronto, Ontario M5S 1A8, Canada

Received October 12, 2015; Revised March 20, 2017; Editorial Decision March 23, 2017; Accepted March 23, 2017

ABSTRACT

In plants, the histone H3.1 lysine 27 (H3K27) monomethyltransferases ARABIDOPSIS TRITHORAX RELATED PROTEIN 5 and 6 (ATXR5/6) regulate heterochromatic DNA replication and genome stability. Our initial studies showed that ATXR5/6 discriminate between histone H3 variants and preferentially methylate K27 on H3.1. In this study, we report three regulatory mechanisms contributing to the specificity of ATXR5/6. First, we show that ATXR5 preferentially methylates the R/F-K*-S/C-G/A-P/C motif with striking preference for hydrophobic and aromatic residues in positions flanking this core of five amino acids. Second, we demonstrate that post-transcriptional modifications of residues neighboring K27 that are typically associated with actively transcribed chromatin are detrimental to ATXR5 activity. Third, we show that ATXR5 PHD domain employs a narrow binding pocket to selectively recognize unmethylated K4 of histone H3. Finally, we demonstrate that deletion or mutation of the PHD domain reduces the catalytic efficiency (k_{cat}/K_m of AdoMet) of ATXR5 up to 58-fold, highlighting the multifunctional nature of ATXR5 PHD domain. Overall, our results suggest that several molecular determinants regulate ATXR5/6 methyltransferase activity and epigenetic inheritance of H3.1 K27me1 mark in plants.

INTRODUCTION

The post-translational modifications (PTMs) of histone proteins are linked to a myriad of nuclear events. Mechanistically, PTMs control chromatin structure or transform histone proteins into selective binding platforms that are recognized by effector proteins. Lysine methylation is an abundant PTM deposited on several residues located on the 'tails' or the globular folds of histone proteins (1). Depending on its specific location on histone proteins, lysine methylation is linked to different biological processes and divergent transcriptional outcomes. Methylation of histone H3 on lysine 9 (H3K9) localizes in regions of the genome that are predominantly transcriptionally silenced while H3K4 methylation is found at the promoter and enhancer regions of actively transcribed genes. In addition to the functional differences associated with specific methyl-lysine residues on histone proteins, lysine ϵ-amine can be mono-, di- or trimethylated (me1/2/3) and each methylation state confers specific functions to chromatin. For instance, chromatin regions enriched in H3K4me1 and H3K4me3 predominantly localize at enhancer and promoter regions, respectively. Analogously, in mouse embryonic stem cells, H3K27me1 accumulates in the intragenic regions of transcribed genes (2) while H3K27me3 co-localizes with the histone variant H3.3 (3) and plays a role in maintaining transcriptionally silenced chromatin domains. Furthermore, H3K27 monomethylation is mostly associated with silencing of transposable elements and other constitutive heterochromatin regions in plants (4,5).

Two functionally non-redundant families of lysine methyltransferases (KMTs) catalyze H3K27 methylation in

*To whom correspondence should be addressed. Tel: +1 613 562 5800 8854; Fax: +1 613 562 5452; Email: jean-francois.couture@uottawa.ca
Present addresses:
Elisa Bergamin, Laboratory of Cell Biology, Howard Hughes Medical Institute, The Rockefeller University, New York, NY 10065, USA.
Jean-Francois Couture, University of Ottawa, Ottawa Institute of Systems Biology, 451 Smyth Road, Roger Guindon Hall, Ottawa, ON K1H 8M5, Canada.

plants. Members of the Polycomb group protein (PcG), CURLY LEAF (CLF), MEDEA (MEA) and SWINGER (SWN) site specifically tri-methylate H3K27 and affect gene imprinting, flowering times and homeotic gene expression (6). In contrast to mammals, in which the PcG proteins EZH1 and EZH2 mono-, di- and tri-methylate H3K27 (2), H3K27me1 is deposited by ARABIDOPSIS TRITHORAX-RELATED PROTEIN 5 and 6 (ATXR5/6) in plants. ATXR5/6 specifically mono-methylate K27 (7) on canonical histone H3.1 (8) and mutations in the *atxr5/6* genes affect the expression of ribosomal RNA gene variants (9), result in replication defects (5) and in the transcriptional activation of repressed regions found in constitutive heterochromatin (7). Collectively, these observations underscore the importance of ATXR5/6 in chromatin structure, transcriptional regulation and DNA replication in plants. ATXR5/6 proteins catalyze lysine methylation through their SET (Suppressor of Variegation 3–9 (Su(var)3–9), Enhancer of Zeste, and Trithorax) domains. Structural studies (8) demonstrated that three loops (referred to as L1, L2 and L3) of the SET domain of ATXR5 bind to histone H3.1 in a L-shaped conformation. The structure also revealed that a region preceding the SET domain of ATXR5 is essential for both the binding and recognition of the histone variant histone H3.1. However, it remains to be determined how ATXR5/6 preferentially methylates K27 on histone H3.1. Furthermore, H3K27 is surrounded by residues that can be covalently modified by other enzymes to influence gene transcription, but the impact of these PTMs on ATXR5 activity is unknown. Lastly, the PHD domain of ATXR5/6 preferentially binds the N-terminus of histone H3.1 when H3K4 is not methylated, however, the structural basis for this discrimination is unknown.

In this study, we describe three mechanisms that allow ATXR5/6 to methylate K27 in constitutive heterochromatic regions. First, we show that ATXR5 SET domain specifically recognizes K27 on histone H3.1 through the stabilization of core residues surrounding its methylation site. Second, we demonstrate that ATXR5 peptide binding cleft tolerates histone H3.1 methylated by ARABIDOPSIS THALIANA Protein Arginine MethylTransferase 4a and 4b (AtPRMT4a and AtPRMT4b) but it is specifically inhibited by PTMs deposited by Increased DNA methylation 1 (IDM1), ARABIDOPSIS THALIANA Protein Kinase 6/9 (ATPK6/19), SET Domain Group 8 (SDG8), on K23, S28 and K36 respectively (10), (11,12). Third, we reveal the crystal structure of ATXR5 PHD domain showing the molecular determinants of the interaction with H3K4. The PHD domain maintains H3K4 ϵ-amine within a narrow pocket highlighting its ability to 'read' H3K4 methylation state. Surprisingly, steady-state kinetic studies show that mutation or deletion of ATXR5 PHD domain does not result in a significant decrease of the K_M of ATXR5 for the nucleosome core particle but affects the binding and the K_M of the enzyme for the cofactor *S*-adenosyl-L-methionine (AdoMet). These observations highlight a novel function of a PHD domain in integrating histone H3 binding, lysine methylation and cofactor binding/release during the catalytic reaction.

MATERIALS AND METHODS

Protein expression and purification

Open reading frames (ORFs), optimized for overexpression in *Escherichia coli*, of *Ricinus communis* and *Glycine max* ATXR5 (RcATXR5 and GmATXR5 respectively) were purchased from GenScript and subcloned in the parallel expression vector pGST2. Full-length GmATXR5 (a.a. 1–334), a GmATXR5 construct lacking the PHD domain (a.a. 105–334, referred to as ATXR5 ΔPHD), the PHD domain of GmATXR5 (a.a. 23–77) and the SET domain of RcATXR5 (a.a. 158–374) were expressed in fusion with a TEV cleavable glutathione-*S*-transferase (GST). The mutant construct GmATXR5 L39W was prepared using a QuikChange Site-Directed Mutagenesis Kit, according to manufacturer instructions (Stratagen). Constructs were verified by DNA sequencing.

RcATXR5 and ATXR5 ΔPHD were expressed and purified as previously described (8). Full-length GmATXR5 was transformed in Rosetta cells (EMD Millipore), and cultures were grown in Luria-Bertani broth media supplemented with 100 μM $ZnCl_2$ at 37°C to an OD_{600} of 0.6. Protein expression was induced by the addition of isopropyl-thiogalactopyranoside (IPTG, 0.2 mM) for 16 h at 19°C. Cells were harvested, resuspended in cold PBS buffer (pH 7.3) and lysed by sonication. The lysate was centrifuged at 37 000 × g for 1 h, and the supernatant was collected. The soluble fraction was incubated with gluthatione sepharose beads for 1 h at 4°C and then washed extensively in PBS buffer. GST-GmATXR5 was TEV cleaved on beads for 16 h at 4°C in a buffer containing 50 mM Tris–HCl (pH 8.0), 500 mM NaCl and 1 mM dithiothreitol (DTT), then concentrated and further purified by gel filtration chromatography (Superdex 200, GE Healthcare). GmATXR5 PHD domain was expressed and purified as described for full-length GmATXR5 with the only exceptions that bacterial pellets were lysed in presence of 10% glycerol to facilitate protein solubilization and the purification by gel filtration chromatography was performed in a buffer composed of 20 mM Tris–HCl (pH 8.0), 200 mM NaCl and 1 mM DTT.

Crystallization and structure determination

The 19-residues peptides corresponding to the region surrounding H3.1 K27 (a.a. 18–36), harboring post-translational modifications KQLATKAAR^{me1}KSAPATGGVKY (R26me1), KQLATKAAR^{me2}KSAPATGGVKY (R26me2a), KQLATKAARKS^{P}APATGGVKY (S28ph), KQLATKAARKSAPATGGVK ^{me3}Y (K36me3), KQLAK^{ac}AARKSAPATGGVKY (K23ac) and the 10-residues peptide representing the N-terminal region of H3.1 (a.a. 1–10, ARTKQTARKSY) encompassing K4, were synthesized by Genscript and solubilized in 100 mM Tris (pH 8.0) and 150 mM NaCl. The peptides carry an additional tyrosine residue at the C-terminus for UV quantification purpose.

Co-crystals of RcATXR5/AdoHcy/H3.1 modified peptides were grown as previously described (8). Briefly, a concentrated solution of RcATXR5 (20 mg/ml) incubated with a 5-fold molar excess of modified H3.1 peptide and

a 2-fold molar excess of S-adenosylhomocysteine (AdoHcy) was mixed (1:1) with the mother liquor composed of 50% polypropylene glycol 400, 5% DMSO, 0.1 M HEPES–NaOH (pH 6.0). Crystals transferred into the mother liquor, were harvested and flash-frozen in liquid nitrogen.

X-ray data were collected using a Marmosaic 300 CCD detector (Rayonix Inc.) at the Life Science Collaborative Access Team (LS-CAT) 21ID-D beamline of the Advanced Photon Source, Argonne National Laboratory, USA. The data were processed and scaled using XDS and aimless, respectively (13,14). A molecular replacement solution was found using Phaser (15) and RcATXR5 structure as a search model (4O30.pdb). The model was completed using interactive rounds of refinement and model building using Buster and Coot, respectively (16,17). Quality of the models was assessed using Molprobity (18) (Supplementary Table S1).

A solution of 45 mg/ml of ATXR5 PHD domain was incubated with the peptide representing the N-terminal region of H3 (a.a. 1–10, ARTKQTARKSY) in a molar excess 1.2:1 of peptide and crystals of the complex were obtained in a condition consisting of 0.1 M HEPES (pH 6.5), 10% PEG 6000 and 5% (±)-2-methyl-2,4-pentanediol. A 1.7 Å resolution data set was collected on a rotating anode source (Rigaku MicroMAX 007-HF, RAXIS-4 image plate detector, VariMax HF optics) and processed using HKL2000 (Otwinowski and Minor, 1997). The crystal structure of ATXR5 PHD domain was solved by molecular replacement using a fragment of the bromodomain adjacent to zinc finger domain protein 2A PHD domain (BAZ2B) (PDB: 4QF3) as a search model using Phaser (19). The model was completed using several rounds of refinement and modeling using Phenix (20) and Coot (21). Quality of the model was assessed using Molprobity (18) (Supplementary Table S1). Coordinates and structure factors for the ATXR5 SET domain in complex with H3.1R26me, H3.1R26me2a, H3.1K36me3 and unmodified histone H3.1 peptides as well as the PHD domain of ATXR5 in complex with histone H3 have been deposited in the protein data bank (rcsb.org) with the accession number 5VA6.pdb, 5VAH.pdb, 5VAC.pdb, 5VBC.pdb and 5VAB.pdb respectively.

Peptide array

Custom peptide arrays printed on trioxatridecanediamine (TOTD) modified cellulose membrane were synthesized by Kinexus (Vancouver, Canada). The peptide sequences, arranged in a 14 × 20 array, were based on the sequence of the H3.1 N-terminal tail around K27 (a.a. 23–36) and represented all possible single amino acid substitutions. AdoMet was obtained from Sigma and radiolabeled [^{3}H-*methyl*]-AdoMet was obtained from Perkin Elmer (17.2 Ci/mmol). The methyltransferase reaction was performed in triplicate incubating the peptide array at 30°C for 60 min with 4 μM of ATXR5 SET domain and AdoMet at a ratio of 2.5 μM: 7.5 μM labeled and un-labeled respectively, in a buffer containing 50 mM Tris (pH 8.5), 20 mM KCl, 10 mM $MgCl_2$, 10 mM β-mercaptoethanol, 10% glycerol, 2% bovine serum albumin (BSA). The reaction was stopped by rinsing the peptide array four times for 5 min in a solution containing 8 M urea, 1% sodium dodecyl sulfate, 0.5 mM β-mercaptoethanol; three times for 5 min in a solution containing 50% ethanol, 10% acetic acid and three times for 2 min in 95% ethanol. The peptide array was dried and imaged using a Typhoon phosphorimager.

Methyltransferase assays

Enzymatic assays of ATXR5 SET domain on histone peptides were performed by scintillography as previously described (8,22,23). Methyltransferase assays performed on octamer and nucleosomes substrates were prepared as follow. The four *xenopus leavis* core histones were co-expressed in *E. coli* and purified in native form by binding on Talon resin (Clontech) and by size exclusion chromatography (Superdex 200, GE Healthcare) (24). The octamer and the 147 base pairs nucleosome positioning 601 DNA (25) were mixed together at a molar ratio of approximately 1:1 in 2 M NaCl, 10 mM Tris (pH 8.0) and nucleosomal assembly was achieved by serial salt dilutions down to 250 mM NaCl (26). Methyltransferase assays were performed with the nucleosome core particles or octamers at 0.2 μM, increasing amounts of ATXR5 full-length, ATXR5 L39W or ATXR5 ΔPHD (0.375, 0.75, 1.5 μM), 1.8 μM radiolabeled [^{3}H-*methyl*]-AdoMet in buffer containing 50 mM Tris (pH 8.5), 20 mM KCl, 10 mM $MgCl_2$, 10 mM β-mercaptoethanol and 10% glycerol in a final volume of 30 μl at 30°C for 1 h. Reactions were stopped by boiling in SDS-PAGE sample buffer and separated by SDS-PAGE. The gels were treated for scintillation, dried, autoradiographed and quantified as previously described (8,22,23).

A radioactivity-based filter plate method was used to determine the kinetic parameters as previously described (27). Tritiated *S*-adenosyl-L-methionine ([^{3}H-*methyl*]-AdoMet; PerkinElmer Life Sciences; catalog no. NET155V250UC) was used as a methyl donor and methylated nucleosome was captured and quantified on filter plate (Millipore; catalog no. MSFBN6B50). The reactions were quenched using trichloroacetic acid (TCA). After adding the scintillant (Microscint-O from PerkinElmer Life Sciences) the radioactivity (counts per minute) was quantified using a TopCount NXT™ Microplate Scintillation and Luminescence Counter (PerkinElmer Life Sciences). The assay mixture (20 μl in volume) contained 50 mM Tris (pH 8.5), 20 mM KCl, 10 mM $MgCl_2$, 10 mM β-mercaptoethanol and 10% glycerol, and 50 nM ATXR5 and various concentrations of AdoMet and nucleosome. The kinetic parameters were determined by varying the concentration of one substrate while keeping the second substrate at saturation.

Electrophoretic mobility shift assays

Nucleosomes were assembled using the salt dilution method with recombinant histone octamers and the 147 bp 601 DNA generated by PCR using primers carrying 5′ Cy5 fluorophore. These labeled probes were incubated at 10 nM in 20 μl binding reactions containing 50 mM Tris–HCl pH 8.5, 20 mM KCl, 10 mM β-mercaptoethanol, 10% (v/v) glycerol and with sinefungin concentrations that reflect the 10X and 1000X-fold compared to the amount of protein used in the binding reactions. Purified ATXR5 full-length, wild-type or L39W mutant, was added to the binding reactions

at varying concentrations, and the reactions were incubated on ice for 30 min. Binding reactions performed with wild-type and mutant AXTR5 were supplemented with 1% and 1.25% BSA, respectively. Samples were then loaded on non-denaturing 4% acrylamide gels (60:1 ratio of acrylamide to bis-acrylamide) containing 10% glycerol, using 0.5× TBE (40 mM Tris–HCl, 45 mM boric acid and 1 mM EDTA) as running buffer. After electrophoresis, gels were immediately scanned using a GE Typhoon Trio Phosphorimager.

Pull-down experiments

GST-PHD and SET domain ATXR5 were prepared as indicated above. ATXR5 GST-PHD crude lysate was incubated with glutathione-*S*-transferase (GST) beads for 1 h at 4°C. The beads were then washed in PBS buffer and further incubated with 100 μg of pure ATXR5 SET domain for 2 h at 4°C in presence or absence of the cofactor analog sinefungin in a buffer consisting of 50 mM Tris (pH 8.5), 20 mM KCl, 10 mM $MgCl_2$, 10 mM β-mercaptoethanol and 10% glycerol in a final volume of 300 μl. The bound sample was washed three times in the same buffer and then beads were boiled in 30 μl of Laemmli buffer.

RESULTS AND DISCUSSION

Substrate specificity

Initial structural studies have shown that ATXR5 peptide binding cleft stabilizes the backbone of residues K23–K36 of histone H3.1 (8) (single letter code refers to histone H3.1 residues and three letters code refers to ATXR5 residues) (Figure 1A and 1B). To investigate the recognition of K27 on histone H3.1 by ATXR5, a 14 amino acids long peptide corresponding to residues K23-K36 (KAARK*SAPATVGGK) of histone H3.1 was systematically substituted to every natural amino acid. The resulting 280 peptides were cross-linked to a cellulose membrane. Three identical arrays were incubated with purified ATXR5 SET domain in the presence of H^3-AdoMet and methylation was quantified by phosphorimaging (Supplementary Figure S1) and represented as a heat map (Figure 1C) or as amino acid binding motif (Figure 1D). Overall, the normalized averaged intensities show three distinct patterns, spanning residues from position –2 to +9 with respect to the target lysine. In pattern I, substitutions do not decrease the activity of ATXR5 and include glycine residues (G33 and G34) occupying positions P^{+6} and P^{+7}. This pair of glycine residues is predominantly solvent exposed in the ATXR5/H3.1/AdoHcy complex but their amide groups make several short hydrogen bonds with ATXR5. These observations suggest that replacement of residues at position P^{+6} and P^{+7} presumably does not perturb the set of hydrogen bonds that forms between the enzyme and its substrate, and advocate in favor of a certain degree of plasticity of ATXR5 P^{+6} and P^{+7} binding pockets (Figure 1C and D).

In contrast to pattern I, the substitutions of residues belonging to pattern II result in a severe loss of ATXR5 methyltransferase activity. Substitution of the arginine and serine residues in positions P^{-1} and P^{+1} to any residues other than a phenylalanine and a cysteine/threonine, respectively, is detrimental to ATXR5 activity. In histone H3.1, R26 occupies the P^{-1} position and likely makes a salt-bridge interaction with Glu365. Moreover, the guanidium group of the same residue in histone H3 is found in a near planar arrangement with the carboxylate group of Glu367. While π-stacking is rarely mentioned in the absence of aromatic moiety, the orientation of R26 and Glu367 suggest that the interaction between these two residues is further stabilized by π-stacking interaction. This hypothesis is further supported by the ability of the enzyme to efficiently methylate peptides substrate harboring an aromatic residue such as phenylalanine in position P^{-1} (Figure 1). In position P^{+1}, S28 hydroxyl group makes a short hydrogen bond with the backbone amide of Glu365 of ATXR5, which possibly explains the negative impact of replacing S28 by small non-polar residues such as a glycine or an alanine. The exquisite selectivity at this position can also be explained by the fact that a loop in ATXR5 SET domain, referred to as safety belt, completely buries S28 and maintains the residue in a constrained pocket (Figure 1A and 1B). Analysis of the substitutions of residues in positions P^{+2} and P^{+3} shows that these residues also belong to pattern II (Figure 1C and 1D). Substitution of A29 and P30 to any other amino acids severely impairs methylation of the peptide substrates by ATXR5. As observed with S28, ATXR5 safety belt cages A29 and P30 which likely limits the repertoire of substitutions accommodated by the enzyme's P^{+2} and P^{+3} binding pockets. Finally, ATXR5 can methylate peptides substituted at position P^{+4} with proline, lysine, serine and glycine residues; however none of these substitutions increases ATXR5 enzymatic activity (Figure 1C and 1D). In contrast to patterns I and II, residues belonging to the third pattern (pattern III), include substitutions that increase ATXR5 activity. Replacement of A24 in P^{-3} position by hydrophobic residues such as an isoleucine, a phenylalanine or a methionine increases methylation by ∼5-folds. Similarly, replacement of A25 in P^{-2} by tryptophan, arginine or large hydrophobic residues generates better substrates for ATXR5 (Figure 1C and 1D). The crystal structure of the ATXR5/H3.1/AdoHcy complex shows that the residue in position P^{-3} binds in a hydrophobic pocket composed of residues found in loop 1 including Met287 side chain and the backbone of Cys284, Asp282 and Glu280 (Figure 1B). Similarly, A25 binds in a solvent-exposed pocket formed by the side chain of Tyr368 and residues found in loops L1 and L3. Residues T32, V35 and K36 are located on the C-terminus of the methylation site, and their substitution shows that the enzyme preferentially methylates substrate with aromatic residues in positions P^{+5}, P^{+8} and P^{+9}. Overall, our results suggest that residues found at the N- and C-termini of the methylation site both contribute to ATXR5 selectivity toward histone H3.1 (Figure 1).

Impact of post-translational modifications on histone H3 K27 mono-methylation

Several residues that surround ATXR5 methylation site on H3.1 are post-translationally modified. For instance, K23 can be acetylated by IDM1, and the presence of this modification antagonizes DNA methylation of heterochromatic loci (10). R26 can be methylated by AtPRMT4 (28), the

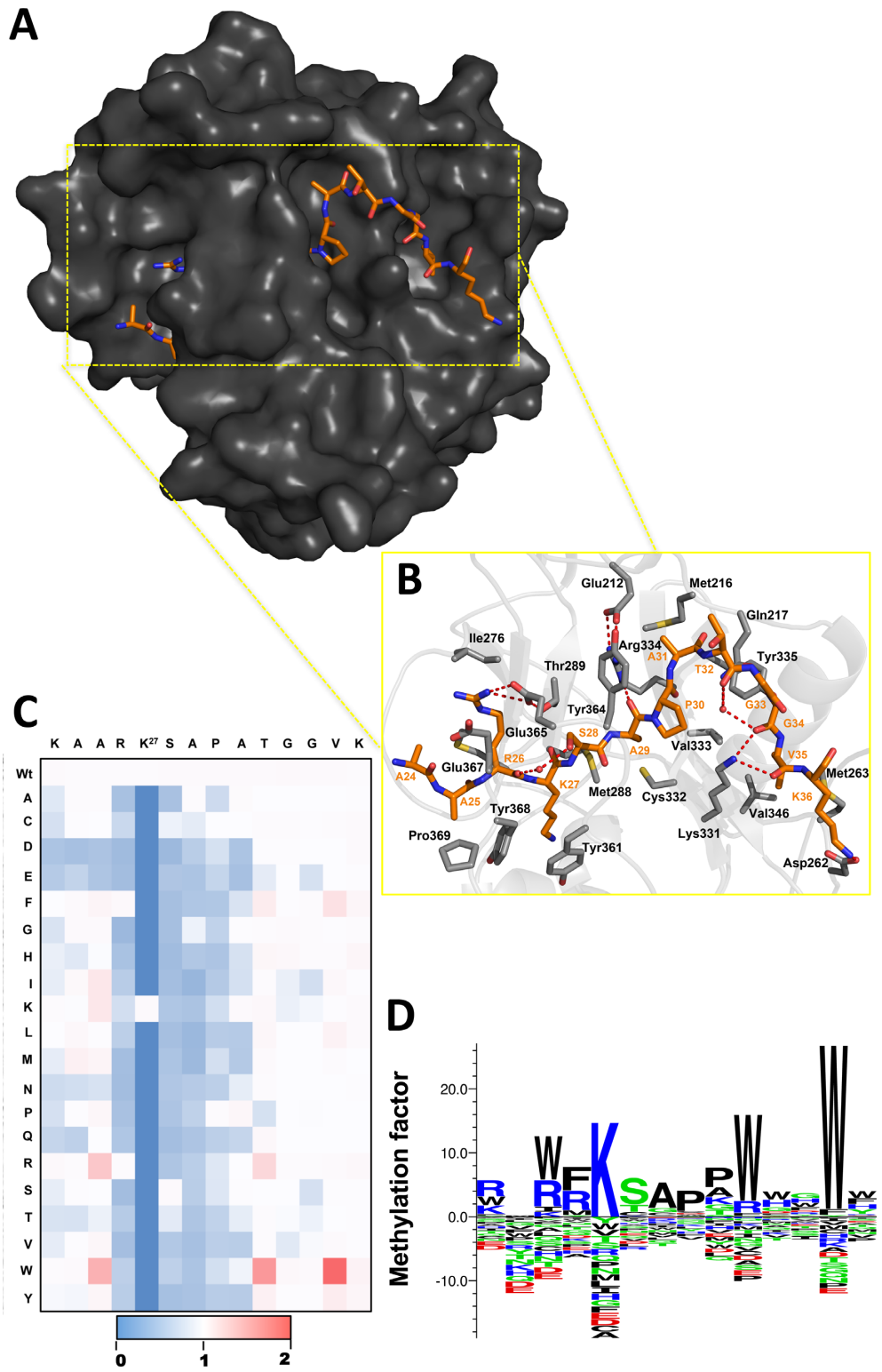

Figure 1. ATXR5 recognizes an extensive motif on H3.1. (**A**) Surface representation of the ATXR5 crystal structure bound to histone H3.1 (revised model of 4o30). The surface of the protein is highlighted in dark gray and the peptide is colored orange. (**B**) Zoomed view representation of ATXR5 binding cleft. ATXR5 and histone H3 residues are rendered in gray and orange residues, respectively. Carbon and oxygen atoms are colored in red and blue respectively. Hydrogen bonds are shown in red dash lines. For clarity, only a subset of the interactions are shown (**C**) Heat map representation of average methylation intensities measured by phosphorimaging shown in Supplementary Figure S1. Color code representing the degree of methylation: white: same methylation intensity as wild type; blue: loss of methylation intensity; red: gain of methylation intensity. (**D**) Sequence logo of the relative methylation factor for every amino acid at each position of the peptide arrays ($n = 3$) performed with the program Seq2logo (http://www.cbs.dtu.dk/biotools/Seq2Logo/), using the PSSM-logo method. Amino acids are sorted from top to bottom in order of importance. Enriched amino acids are represented on the positive y-axis and depleted amino acids are shown in the negative y-axis. Color code: blue: positively charged; red: negatively charged; green: polar; black: all other amino acids.

homolog of human CARM1 (29). Additionally, S28 can be phosphorylated by the protein kinases ATPK6/19 (30), (11), the homolog of mammalian MSK1, and this PTM has recently been suggested to govern the extent and rate of mitotic polycomb dissociation in mammalian stem cells (31–33). Finally, SDG8 and SDG26, homologs of the mammalian SETD2, methylate K36 in the body of genes (Figure 2A) (34–36). In budding yeast, this mark has been shown to serve as a binding site for the histone deacetylase Rpd3 to prevent cryptic transcription (37,38).

To determine the effect of the PTMs deposited near the target site of ATXR5 on the histone tail, we assayed the methyltransferase activity of ATXR5 SET domain with 14-residue histone H3.1 peptides bearing each of the PTMs. As illustrated in Figure 2B, K23 acetylation is detrimental to ATXR5 activity. Interestingly, owing to the lack of electronic density, the side chain of this residue was not modeled in the ATXR5/H3.1/AdoHcy structure. Moreover, H3K23 is positioned relatively far from enzyme's substrate binding cleft, suggesting that the ATXR5/H3.1/AdoHcy structure fails to portray the impact of K23 acetylation on ATXR5 activity. However, our finding that the mark deposited by IDM1 (10) (Figure 2A) blocks the activity of ATXR5 is consistent with an earlier report showing that ATXR5 and DNA methylation cooperate to silence transposable elements (39), and reinforces the notion that there is a tight connection between the transcriptional regulatory mechanisms that involve DNA and histone methylation.

Next we sought to measure the activity of ATXR5 toward mono- and asymmetrically di-methylated H3R26 peptides (R26me1 and R26me2a). Methyltransferase assays with ATXR5 and R26me1 and R26me2a peptides show that the activity of ATXR5 is not affected by R26me1 but reduced by ∼3-fold when R26 is asymmetrically dimethylated (Figure 2B). In the crystal structure of histone H3.1 bound to ATXR5 (8), the H3R26 side chain makes two hydrogen bonds with the carboxylate group of Glu365 (Figure 2C). Closer inspection of H3R26 binding pocket reveals that the addition of a methyl group would create steric clashes with the side chain of Glu365. Therefore, to understand the structural basis underlying the methylation of histone H3.1R26me1 and H3.1R26me2a, we solved the crystal structure of ATXR5 bound to these peptides and AdoHcy at 2.45 and 2.4 Å (Figure 2D and E). Both complexes align well with the crystal structure of the ATXR5/H3.1 complex (PDB: 4O30) with a root mean square deviations of ∼0.192 and 0.189 Å suggesting that H3.1R26me1 and H3.1R26me2a do not induce large structural reorganization of ATXR5 SET domain. However, comparative analysis of both complexes with the structure of ATXR5/H3.1 complex shows that both R26me1 and R26me2a side chains undergo similar structural rearrangements to make novel hydrogen bonds with Glu365 and Thr289 carboxylate and hydroxyl groups, respectively (Figure 2D and E). While the structural data support our observations that unmodified and R26me1 histone H3.1 peptides are methylated at a similar level, it fails to explain the loss of activity H3.1R26me2a peptide. At least two scenarios can be envisioned. Addition of a second methyl group to R26 may slightly change the resonance of its guanidine group, which negatively impacts the ability of this residue to make π interactions. This hypothesis is further supported by the results obtained with the peptide array showing that the aromatic residue phenylalanine is accommodated by ATXR5 peptide binding cleft. Alternatively, dimethylation of R26 may affect the trajectory of the H3.1R26me2a peptide during the binding of the substrate to ATXR5. Overall our results suggest that ATXR5 P^{-1} binding pocket tolerates, with however less activity on H3.1R26me2a, the PTM deposited by AtPRMT4.

Next, we evaluated the effects of S28 phosphorylation (H3S28ph) and K36 tri-methylation (H3K36me3), modifications deposited by ATPK6/19 and SGM8/26 respectively. The methyltransferase assays performed with ATXR5 SET domain and either H3S28ph or H3K36me3 peptides show that the activity of ATXR5 is dramatically impaired when S28 is phosphorylated and it is reduced of approximately three folds when K36 is tri-methylated by SGM8/26 (Figure 2B). The detrimental impact of S28 phosphorylation is consistent with the motif determined using the peptide array, which revealed that charged and bulky residues are not tolerated by the enzyme in P^{+1} position. In addition, close inspection of the ATXR5/H3.1/AdoHcy crystal structure (8) shows that within ATXR5 peptide binding cleft, S28 is completely buried by a loop that presumably impedes the binding of phosphorylated substrates in P^{+1} position (Figure 2F). In the ATXR5/H3.1/AdoHcy complex (8), K36 ϵ-amine makes two short hydrogen bonds with the ATXR5 peptide binding cleft (Figure 2G), which may underlie the negative impact of K36me3 on ATXR5 activity. However, to gain a better understanding of this PTM, we solved the crystal structure of ATXR5 SET domain in complex with a H3.1 peptide carrying the K36me3 modification. The ATXR5/H3.1K36me3/AdoHcy complex aligns well with the structure of ATXR5 in complex with the unmodified H3.1 peptide (PDB: 4O30) with a root mean square deviations of ∼0.190 Å suggesting that this PTM does not induce large structural reorganization of ATXR5 SET domain. Interestingly, in the crystal structure of ATXR5/H3.1K36me3/AdoHcy, no electron density can be observed for K36me3. Moreover, comparative analysis between ATXR5/H3.1K36me3/AdoHcy and ATXR5/H3.1/AdoHcy complexes show that V35 side chain of histone H3.1, which is buried in an hydrophobic pocket composed of Leu161, Val346 and Met263 in the structure of ATXR5 solved in complex with the unmodified histone H3.1 peptide, is displaced by ∼1 Å outside of the aliphatic pocket which results in a reduced numbers of hydrophobic contacts between this residue and ATXR5 peptide binding pocket (Figure 2G). These differences are not due to differences in crystal symmetries as the analyzed peptide is not involved in the crystal packing. These observations suggest that K36 tri-methylation prevents the formation of hydrogen bonds and forces K36 (in P^{+8}), as well as the residue in position P^{+7} out of the ATXR5 peptide binding cleft (Figure 2G). Overall these results demonstrate that ATXR5 activity is reduced by PTMs associated with actively transcribed chromatin (H3K26me2a and H3K36me3), regulating heterochromatin formation (H3S28ph), or marking loci for escaping heterochromatic silencing (H3K23ac). Together, these findings reveal the existence of a second layer of regulation of ATXR5 activity, wherein histone PTMs act in combination with pref-

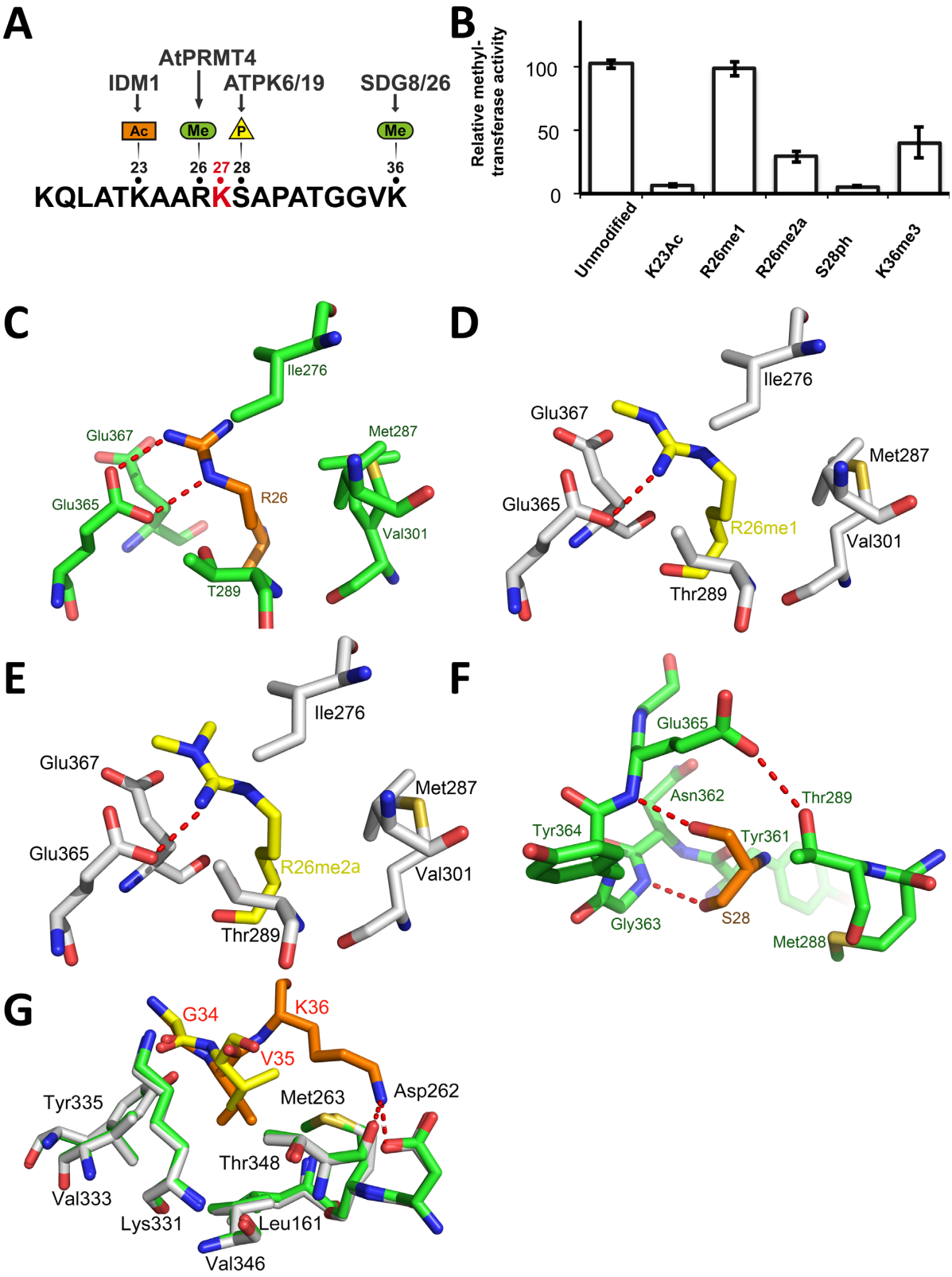

Figure 2. Post-translational modifications of residues neighboring histone H3.1 K27 are detrimental to ATXR5 enzymatic activity. (**A**) Schematic representation of the H3.1 peptide showing the PTMs deposited in vicinity of the K27 methylation site (red). (**B**) Methyltransferase activity of ATXR5 SET domain on modified histone H3.1 peptides relative to un-modified H3.1. (**C**) Zoomed-view of ATXR5 SET domain binding cleft showing un-modified S28 (left) in which the carbon atoms of the peptides and proteins are colored in orange and green respectively. (**D**) Comparison of ATXR5/H3.1/AdoHcy with ATXR5/H3.1K36me3/AdoHcy in which the carbon atoms for the modified peptides and co-crystallized ATXR5 are colored in yellow and white, respectively. Zoomed-view of ATXR5 SET domain binding cleft showing un-modified R26 (**E**), R26me1 (**F**) and R26me2a (**G**). Carbon atoms of the un-modified and modified peptides are rendered in orange and yellow respectively. Hydrogen bonds are highlighted by red dashed lines.

erence for the histone variant H3.1 to control K27 monomethylation.

The role of ATXR5 PHD domain

ATXR5 PHD domain has been shown previously to bind preferentially to the N-terminal tail of histone H3 when it is not tri-methylated on K4 (5), supporting the model wherein PTMs typically associated to gene activation inhibit ATXR5 activity. Interestingly, though apparently independently from the catalytic domain, the PHD domain is essential for K27 methylation and heterochromatin silencing *in vivo* (5), suggesting that the PHD domain is integral to the activity of ATXR5 and constitutes an additional level of control for this enzyme. It also suggests the possibility of a combinatorial action of histone PTM 'reader' and 'writer' domains within ATXR5. To gain a better understanding of the molecular basis of recognition of ATXR5 substrate, we determined the crystal structure of ATXR5 PHD domain (residues 23–77) bound to the unmodified histone H3 tail (residues 1–10, ARTKQTARKS). The crystal structure reveals that ATXR5 PHD domain adopts a canonical 'cross-braced' PHD domain architecture with two loops (loop-1 and loop-2) containing the Cys_4-His-Cys_3 motif that coordinates two zinc atoms, a double-stranded twisted antiparallel β-sheet and two short 3_{10} α-helices (Figure 3A).

In the crystal structure, the 10-residue histone peptide is well ordered (Supplementary Figure S2). The peptide adopts a L-shaped conformation and the specificity of binding is determined primarily by the unique coordination of A1, R2 and K4 by the PHD domain. An extensive network of interactions secures the binding of the first two residues of the peptide to the PHD domain. The free amino group of A1 forms hydrogen bonds with the backbone carbonyl groups of Gly62 and Pro60 located on loop-2 (Figure 3B). The guanidium group of R2 makes electrostatic interactions with Asp41 and Asp44 side chains (Figure 3B). The ϵ-amine of K4 forms hydrogen bonds with the main chain carbonyl oxygens of Val23 and Gly31 located on loop-1 of the PHD domain. Additionally, the amide group of K4 engages in a hydrogen bond with the carbonyl group of Leu37 located on the β1 sheet of the PHD domain (Figure 3B). These three residues create a shallow hydrophobic pocket that accommodates K4. Adjacent to this pocket, Pro34 carbonyl group forms a hydrogen bond with residue Q5. In this region, the peptide makes a sharp turn and projects away from the PHD domain. The turn is stabilized by hydrogen bonds between T3 hydroxyl group and the backbone carbonyl groups of T6 and T3. The side chain of the same residue is accommodated in a shallow pocket defined by Val59 and Ser35.

PHD and SET domains cooperate into mediating ATXR5 function

After determining the structure of ATXR5 PHD domain in complex with the N-terminus of histone H3.1, we sought to gain a better understanding of the role of the PHD domain in ATXR5 lysine methyltransferase (KMTase) activity. We performed KMTase assays comparing the activity of ATXR5 lacking the PHD domain (ATXR5 ΔPHD) with that of the full-length protein. The assays were performed concurrently on histone octamers and on nucleosome core particles (NCPs). These experiments allowed us to make two interesting observations. First, we observed that ATXR5 preferentially methylates NCPs over octamers (Figure 4A, compare lanes 6, 7 and 8 with 13, 14 and 15). This finding is consistent with the fact that ATXR5/6 act during replication to perpetuate the heterochromatin state, and may represent a way to ensure that H3K27me1 will not be deposited erroneously on free histones that would risk being subsequently incorporated into chromatin at transcriptionally active genes (8). Second, we observed that the full-length enzyme is markedly more active compared to ATXR5 ΔPHD, on both octamers and NCPs (Figure 4A, compare lanes 3, 4 and 5 with 10, 11 and 12), suggesting that the PHD domain is important for ATXR5 maximal activity. To confirm that the PHD domain is important for ATXR5 enzymatic activity, we repeated the KTMase assay with an ATXR5 mutant in which L39, a residue located in the PHD domain and implicated in the formation of histone H3 binding pocket, is substituted by a tryptophan residue; this mutation is known to impair the binding of ATXR5 PHD domain to histone H3 (5). As shown in Figure 4B, we observed a loss of methyltransferase activity and confirmed that a functional PHD domain is required for full enzymatic activity.

Based on these observations, we reasoned that histone H3 recognition by ATXR5 PHD domain contributes to the activity of ATXR5 by increasing its binding affinity to the substrate nucleosome. To verify this hypothesis, we determined the kinetic parameters of ATXR5 WT, ATXR5 ΔPHD and ATXR5 L39W for the methylation of the nucleosome. As shown in Figure 5A and consistent with our initial results, the data indicate that both ATXR5 L39W mutant and ATXR5 ΔPHD show reduced methyltransferase activity. However, the K_m value for the nucleosome was unaffected upon mutation or deletion of the PHD domain (Figure 5A–E) but the K_m values for AdoMet increased by 3- and 12-fold for ATXR5 L39W and ΔPHD respectively in comparison with the wild-type ATXR5 (Figure 5C–E) suggesting that the PHD domain is important for AdoMet binding. EMSAs using fluorescently labeled nucleosomes revealed that ATXR5 binds the NCP with an equilibrium dissociation constant of ∼380 nM (Supplementary Figure S5), a K_d that is ∼20-fold less than the concentration of NCP used in our enzymatic assays, suggesting that the inability of ATXR5 mutants to methylate the NCP stems from their inability to bind the cofactor. To confirm that the mutation of ATXR5 PHD domain impairs the binding of the cofactor, we performed EMSAs with Cy5-labeled NCP in presence of an excess (10X or 1000X) of the AdoMet analog sinefungin. Considering that other SET domain methyltransferase require the presence of the cofactor to bind their substrate, we posited that by increasing the concentration of sinefungin, the mutant would show NCP binding activity similar to wild-type ATXR5. Interestingly, a 100-fold difference in sinefungin concentration did not significantly impact the NCP binding activity of wild-type ATXR5 (Figure 6A and 6C). Conversely, consistent with our hypothesis, experiments performed with ATXR5 L39W revealed that in presence of 1000X sinefungin, the mutant showed equiva-

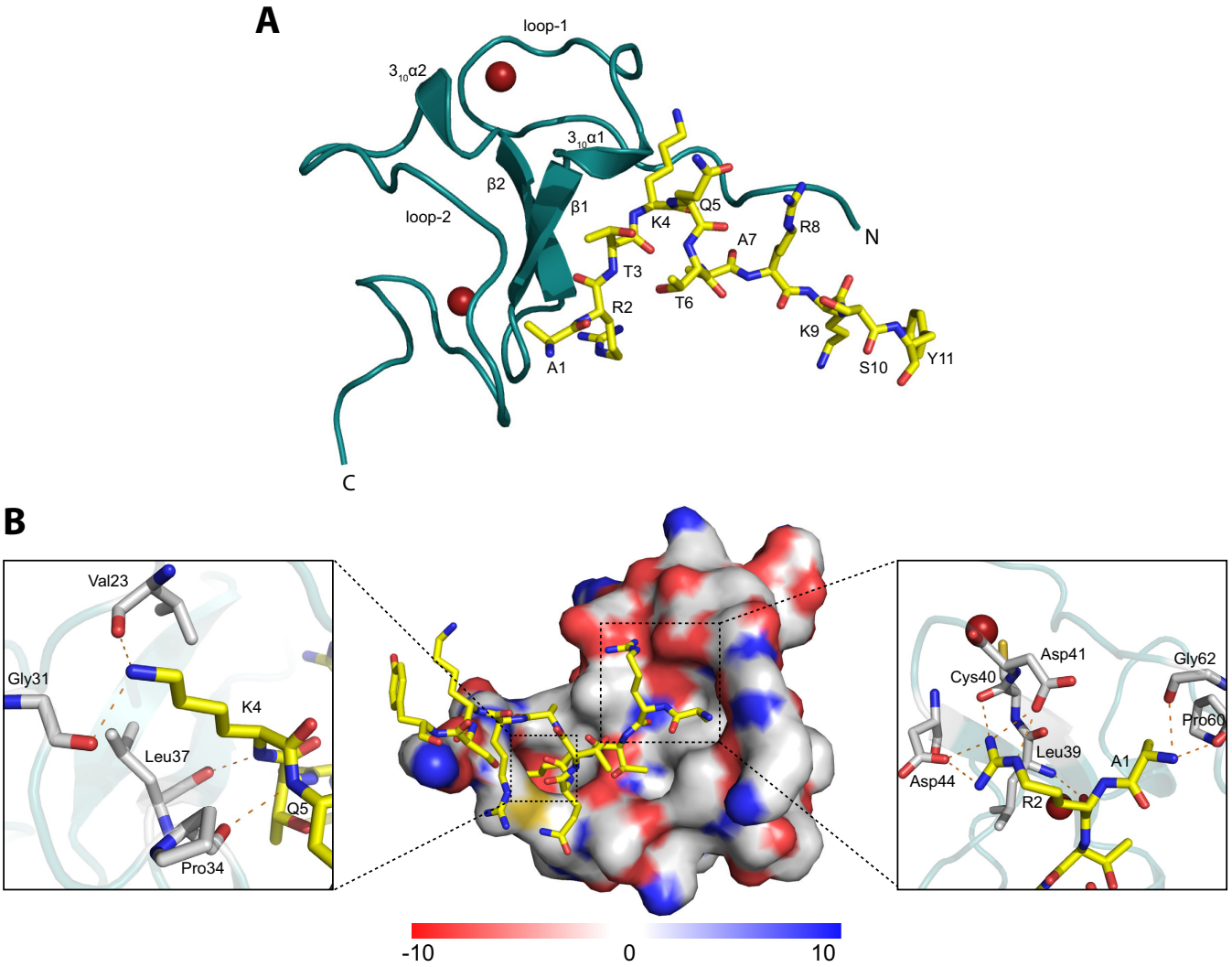

Figure 3. Structure of ATXR5 PHD domain in complex with H3K4 peptide. (**A**) ATXR5 PHD domain is shown in ribbon representation and colored teal. Secondary structure elements (α helices, β strands and loops) are indicated. The N and C termini of the PHD domain are also indicated. Zn atoms are shown as red spheres. The H3K4 peptide is shown in stick representation with carbon atoms colored yellow, oxygen atoms red, nitrogen atoms blue. Figure was rendered with PyMOL (http://pymol.org). (**B**) Molecular surface representation of the ATXR5 PHD domain colored according to electrostatic potential (blue, positive [+10 kT/e]; white, neutral; red, negative [−10 kT/e]). The H3K4 peptide is shown in stick representation and coloring scheme is the same as in (A). Inlet figures show a zoomed view of the residues interacting with K4 (left panel) and with A1 and R2 (right panel). The electrostatic surface representation was made using the Adaptive Poisson Boltzmann Equation (APBS) plugin in PyMOL (44).

lent activity to the wild-type enzyme. Altogether, these results suggest that ATXR5 PHD domain is important for the high affinity binding of the cofactor. To confirm this hypothesis, GST tagged PHD was incubated with ATXR5 SET domain in presence or absence of the cofactor analog sinefungin. Following affinity purification on glutathione sepharose beads, proteins were separated on a denaturating SDS-PAGE gel and stained with coomassie brilliant blue. As shown in Figure 6E, in absence of sinefungin, binding of ATXR5 SET domain to GST-PHD is not detected. However, consistent with the methyltransferase assays, specific binding of ATXR5 SET domain to its PHD domain was observed in presence of sinefungin. These results strongly suggest that the PHD domain of ATXR5 senses the binding of sinefungin to the SET domain.

The results of the EMSAs and kinetic assays show that ATXR5 PHD domain contributes to the binding of the cofactor and play a minimal role in the interaction of the enzyme with the NCP in presence of saturating concentration of sinefungin. While these results strongly suggest that the histone H3 binding activity of ATXR5 PHD domain in the context of the NCP is accessory, they can be perceived as contradictory to the crystal structure of ATXR5 PHD domain in complex with the N-terminus of histone H3 which shows that the zinc finger engages in several electrostatic interactions with histone H3. One possibility is that during DNA replication, the PHD domain of ATXR5 senses the methylation state of histone H3 prior its deposition onto chromatin. Analogously, in a model wherein histone proteins in front of the replication fork are recycled and redeposited following DNA duplication, the PHD do-

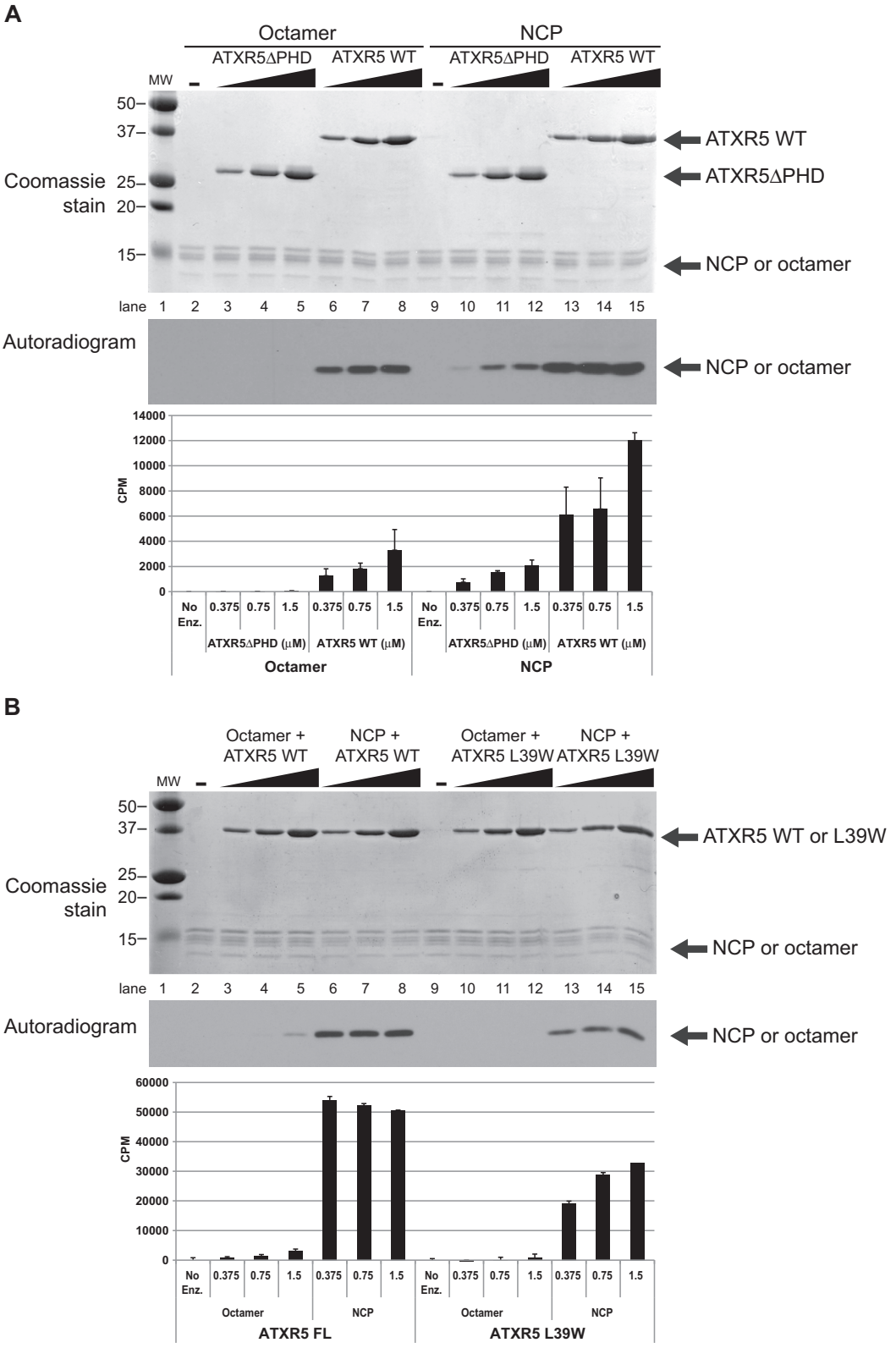

Figure 4. ATXR5 activity is stronger on the NCP and with an intact PHD domain. KMTase assays were performed using histone octamers or NCP as substrate, using tritiated S-adenosyl-L-Methionine and varying amounts of WT or mutant enzyme. (**A**) Reactions performed with ATXR5 WT or a mutant in which the PHD domain has been deleted. Reaction products were separated by SDS-PAGE, gel extracted using isopropanol and radioactivity on histones was quantitated by scintillography. (**B**) Similar reactions were performed, this time comparing ATXR5 WT or L39W mutant. Reactions were stopped by spotting the reactions on P81 filter paper and quantified by scintillography.

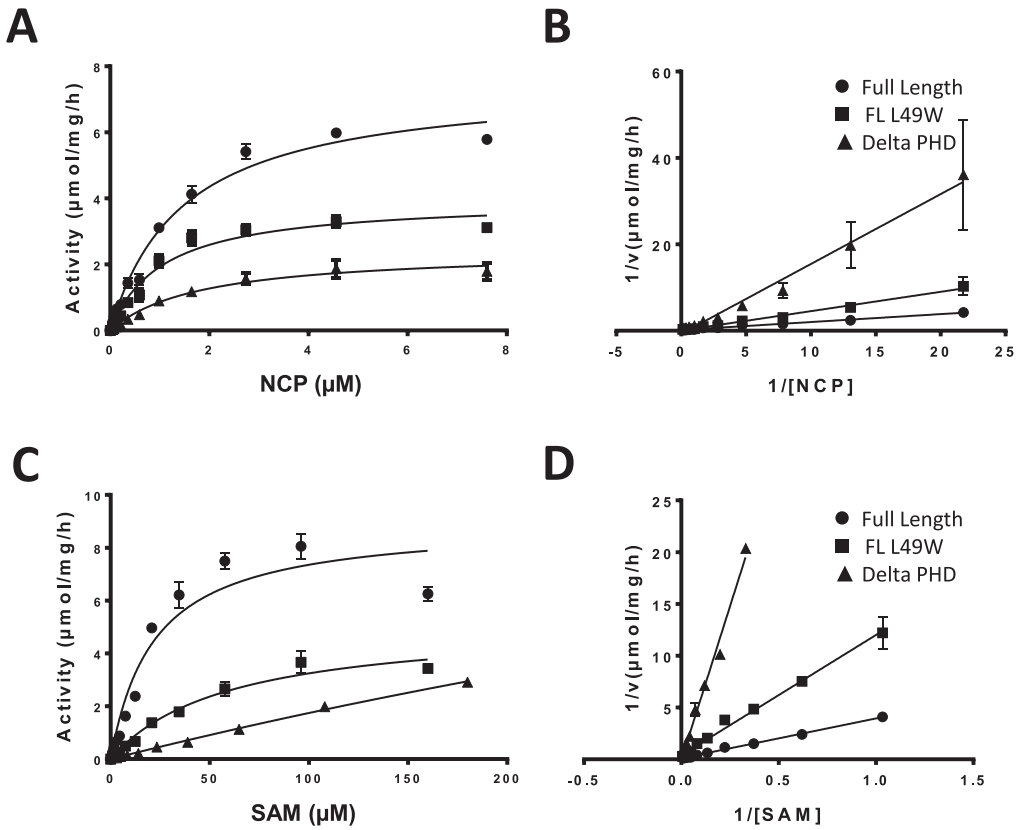

E

Kinetic characterization of wild-type and mutant ATXR5

ATXR5	K_m^{app} (µM)		k_{cat} (h^{-1})	k_{cat} / $K_{m\ SAM}$ (h^{-1} μM^{-1})
	Nucleosome	SAM		
wild-type	1.5 ± 0.1	16 ± 1	280 ± 6	17.5
L49W	1.1 ± 0.1	45 ± 3	146 ± 3	3.2
ΔPHD	1.9 ± 0.3	192 ± 20	64 ± 8	0.3

Figure 5. Cofactor steady-state kinetics are affected by the mutation of ATXR5 PHD domain. Michaelis–Menten (M–M) plot of the initial velocity versus nucleosome concentration (**A**) and its Lineweaver–Burk (LB) double reciprocal plot (**B**) for full-length wild-type ATXR5, L39W mutant and ATXR5 ΔPHD. The kinetics for the cofactor were performed using 8 µM of recombinant nucleosome. The M-M plot of the initial velocity versus cofactor concentration (**C**) and its corresponding LB plot (**D**) for the constructs used in C. (**E**) Summary of the results obtained from the M-M plots for wild-type ATXR5, L39W mutant and ATXR5 ΔPHD.

main would serve as a domain restricting the deposition of histone H3.1 molecules that are not methylated on K4 only. Once deposited, the PHD domain would either stay bound to or dissociate from histone H3.1 to fold back onto ATXR5 cofactor binding cleft to stabilize S-Adenosyl-L-methionine. While the roles of PHD domains in regulating the recruitment of proteins to chromatin are well documented (40,41), this is the first report highlighting the role of a PHD domain in contributing to the K_m of the cofactor for an enzyme (Figure 6F). Interestingly, our findings are reminiscent of what occurs with the H3K9 methyltransferase Suv39H1. Deletion or mutation of Suv39H1 chromodomain, located on the N-terminus of its SET domain, greatly diminishes its enzymatic activity (42). Overall, these results indicate that the PHD domain is needed for the SET domain's ability to bind the cofactor and to monomethylate K27 of histone H3.1.

In conclusion, our findings suggest the existence of multiple regulatory mechanisms that strongly restrict the silencing activity of ATXR5: not only the enzyme will be inactive if nucleosomes carry H3.3 (8), but it will also be inefficient if PTMs typical of euchromatin are present near H3K27. Further, through a modulation of the affinity for S-Adenosyl-L-Methionine and its ability to recognize histone H3 when K4 is unmethylated, the PHD domain will ensure that the enzyme does not establish the silent chromatin mark H3K27me1 if a locus is marked by H3K4me3. This is consistent with *in vivo* data showing a strong genome-

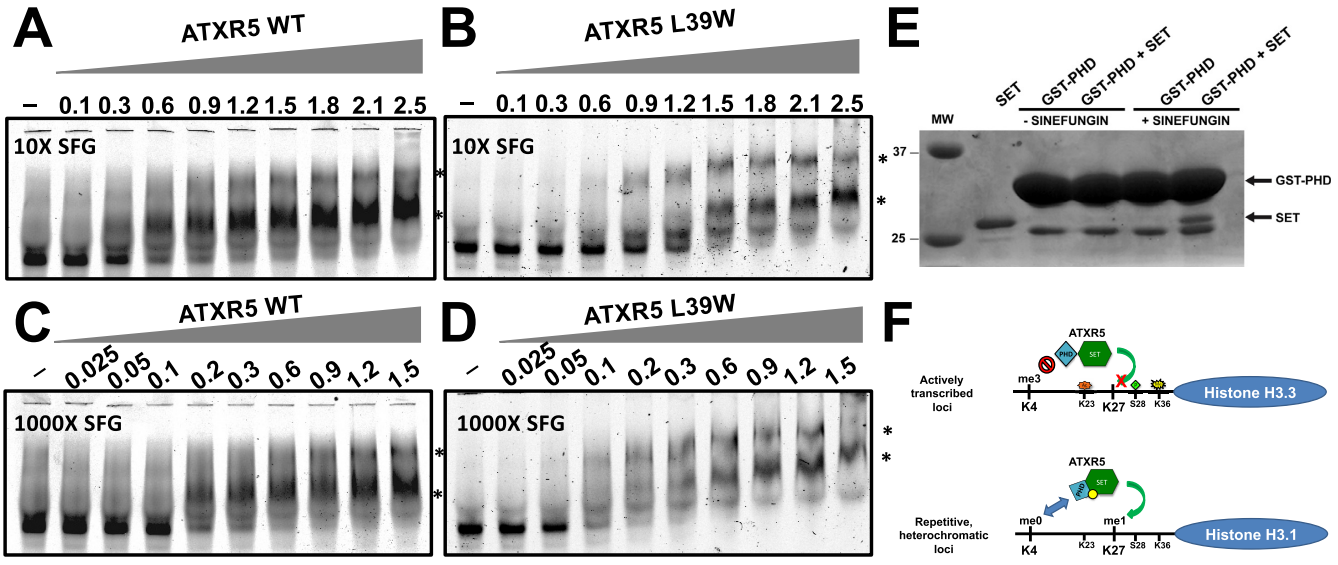

Figure 6. Increasing cofactor concentration bypasses the inability of ATXR5 mutant to bind the nucleosome. EMSA experiments were performed by incubating increasing amounts of ATXR5 WT in presence of 10X (**A**) or 1000X (**C**) of sinefugin (SFG) and fixed amounts of fluorescently-labeled NCP. Similar EMSAs were performed with ATXR5 L39W in 10X (**B**) or 1000X (**D**). Reactions were resolved on non-denaturing polyacrylamide gels. The * indicates the ATXR5–NCP complexes and the protein concentrations are indicated on the top of each gel. (**E**) GST pull-down assays showing the interaction between ATXR5 PHD domain with untagged ATXR5 SET domain in presence of sinefugin. Proteins were resolved on a denaturating SDS-PAGE gel and stained with Coomassie Brilliant Blue. (**F**) Model of the regulatory elements controlling the activity of ATXR5. The SET and PHD domains of ATXR5 are colored in green and blue respectively and are shown in two different conformations on active (top) or silent (bottom) chromatin and the cofactor is represented by a yellow circle. Histone tails of H3.3 and H3.1 are shown as black lines and the residues with their respective PTMs are indicated.

wide anti-correlation between the presence of H3K27me1, deposited by ATXR5/6, and H3K4me3, a mark deposited by ATX1 and ATX2 at expressed loci (5,43). Finally, it is tempting to speculate that a conformational change occurs in ATXR5 that brings the SET and PHD domains in close proximity in presence of cofactor. The concentration of cofactor in the cell could potentially trigger ATXR5 structural rearrangement and therefore constitute an additional layer of regulation of ATXR5 activity. We therefore propose that the combinatorial action of these regulatory mechanisms restricts the mitotic inheritance of heterochromatin to silent heterochromatic loci and protect transcriptionally active genes against silencing (Figure 6F).

SUPPLEMENTARY DATA

Supplementary Data are available at NAR Online.

ACKNOWLEDGEMENTS

We would like to thank Anthony Semesi for nucleosome preparation.

FUNDING

Natural Sciences and Engineering Research Council (NSERC) discovery grant (awarded to J. -F.C.); J. -F.C. holds a Canada Research Chair in Structural Biology and Epigenetics; The SGC is a registered charity [1097737] that receives funds from AbbVie, Bayer Pharma AG, Boehringer Ingelheim, Canada Foundation for Innovation, Eshelman Institute for Innovation, Genome Canada, Innovative Medicines Initiative (EU/EFPIA) [ULTRA-DD 115766], Janssen, Merck & Co., Novartis Pharma AG, Ontario Ministry of Economic Development and Innovation, Pfizer, São Paulo Research Foundation-FAPESP, Takeda and the Wellcome Trust. Funding for open access charge: Natural Sciences and Engineering Research Council (NSERC) discovery grant awarded to J. -F.C.
Conflict of interest statement. None declared.

REFERENCES

1. Lanouette,S., Mongeon,V., Figeys,D. and Couture,J.F. (2014) The functional diversity of protein lysine methylation. *Mol. Syst. Biol.*, **10**, 724.
2. Ferrari,K.J., Scelfo,A., Jammula,S., Cuomo,A., Barozzi,I., Stutzer,A., Fischle,W., Bonaldi,T. and Pasini,D. (2014) Polycomb-dependent H3K27me1 and H3K27me2 regulate active transcription and enhancer fidelity. *Mol. Cell*, **53**, 49–62.
3. Goldberg,A.D., Allis,C.D. and Bernstein,E. (2007) Epigenetics: a landscape takes shape. *Cell*, **128**, 635–638.
4. Roudier,F., Ahmed,I., Berard,C., Sarazin,A., Mary-Huard,T., Cortijo,S., Bouyer,D., Caillieux,E., Duvernois-Berthet,E., Al-Shikhley,L. *et al.* (2011) Integrative epigenomic mapping defines four main chromatin states in Arabidopsis. *EMBO J.*, **30**, 1928–1938.
5. Jacob,Y., Stroud,H., Leblanc,C., Feng,S., Zhuo,L., Caro,E., Hassel,C., Gutierrez,C., Michaels,S.D. and Jacobsen,S.E. (2010) Regulation of heterochromatic DNA replication by histone H3 lysine 27 methyltransferases. *Nature*, **466**, 987–991.
6. Wood,C.C., Robertson,M., Tanner,G., Peacock,W.J., Dennis,E.S. and Helliwell,C.A. (2006) The Arabidopsis thaliana vernalization response requires a polycomb-like protein complex that also includes VERNALIZATION INSENSITIVE 3. *Proc. Natl. Acad. Sci. U.S.A.*, **103**, 14631–14636.
7. Jacob,Y., Feng,S., LeBlanc,C.A., Bernatavichute,Y.V., Stroud,H., Cokus,S., Johnson,L.M., Pellegrini,M., Jacobsen,S.E. and Michaels,S.D. (2009) ATXR5 and ATXR6 are H3K27

monomethyltransferases required for chromatin structure and gene silencing. *Nat. Struct. Mol. Biol.*, **16**, 763–768.
8. Jacob,Y., Bergamin,E., Donoghue,M.T., Mongeon,V., LeBlanc,C., Voigt,P., Underwood,C.J., Brunzelle,J.S., Michaels,S.D., Reinberg,D. *et al.* (2014) Selective methylation of histone H3 variant H3.1 regulates heterochromatin replication. *Science*, **343**, 1249–1253.
9. Pontvianne,F., Abou-Ellail,M., Douet,J., Comella,P., Matia,I., Chandrasekhara,C., Debures,A., Blevins,T., Cooke,R., Medina,F.J. *et al.* (2010) Nucleolin is required for DNA methylation state and the expression of rRNA gene variants in Arabidopsis thaliana. *PLoS Genet.*, **6**, e1001225.
10. Qian,W., Miki,D., Zhang,H., Liu,Y., Zhang,X., Tang,K., Kan,Y., La,H., Li,X., Li,S. *et al.* (2012) A histone acetyltransferase regulates active DNA demethylation in Arabidopsis. *Science*, **336**, 1445–1448.
11. Cerutti,H. and Casas-Mollano,J.A. (2009) Histone H3 phosphorylation: universal code or lineage specific dialects? *Epigenetics*, **4**, 71–75.
12. Liu,C., Lu,F., Cui,X. and Cao,X. (2010) Histone methylation in higher plants. *Annu. Rev. Plant Biol.*, **61**, 395–420.
13. Kabsch,W. (2010) Xds. *Acta Crystallogr. D Biol. Crystallogr.*, **66**, 125–132.
14. Evans,P.R. and Murshudov,G.N. (2013) How good are my data and what is the resolution? *Acta Crystallogr. D Biol. Crystallogr.*, **69**, 1204–1214.
15. Zwart,P.H., Afonine,P.V., Grosse-Kunstleve,R.W., Hung,L.W., Ioerger,T.R., McCoy,A.J., McKee,E., Moriarty,N.W., Read,R.J., Sacchettini,J.C. *et al.* (2008) Automated structure solution with the PHENIX suite. *Methods Mol. Biol.*, **426**, 419–435.
16. Blanc,E., Roversi,P., Vonrhein,C., Flensburg,C., Lea,S.M. and Bricogne,G. (2004) Refinement of severely incomplete structures with maximum likelihood in BUSTER-TNT. *Acta Crystallogr. D Biol. Crystallogr.*, **60**, 2210–2221.
17. Emsley,P., Lohkamp,B., Scott,W.G. and Cowtan,K. (2010) Features and development of Coot. *Acta Crystallogr. D Biol. Crystallogr.*, **66**, 486–501.
18. Davis,I.W., Leaver-Fay,A., Chen,V.B., Block,J.N., Kapral,G.J., Wang,X., Murray,L.W., Arendall,W.B. 3rd, Snoeyink,J., Richardson,J.S. *et al.* (2007) MolProbity: all-atom contacts and structure validation for proteins and nucleic acids. *Nucleic Acids Res.*, **35**, W375–383.
19. McCoy,A.J., Grosse-Kunstleve,R.W., Adams,P.D., Winn,M.D., Storoni,L.C. and Read,R.J. (2007) Phaser crystallographic software. *J. Appl. Crystallogr.*, **40**, 658–674.
20. Adams,P.D., Afonine,P.V., Bunkoczi,G., Chen,V.B., Echols,N., Headd,J.J., Hung,L.W., Jain,S., Kapral,G.J., Grosse Kunstleve,R.W. *et al.* (2011) The Phenix software for automated determination of macromolecular structures. *Methods*, **55**, 94–106.
21. Emsley,P. and Cowtan,K. (2004) Coot: model-building tools for molecular graphics. *Acta Crystallogr. D Biol. Crystallogr.*, **60**, 2126–2132.
22. Avdic,V., Zhang,P., Lanouette,S., Groulx,A., Tremblay,V., Brunzelle,J. and Couture,J.F. (2011) Structural and biochemical insights into MLL1 core complex assembly. *Structure*, **19**, 101–108.
23. Avdic,V., Zhang,P., Lanouette,S., Voronova,A., Skerjanc,I. and Couture,J.F. (2011) Fine-tuning the stimulation of MLL1 methyltransferase activity by a histone H3-based peptide mimetic. *FASEB J.*, **25**, 960–967.
24. Shim,Y., Duan,M.R., Chen,X., Smerdon,M.J. and Min,J.H. (2012) Polycistronic coexpression and nondenaturing purification of histone octamers. *Anal. Biochem.*, **427**, 190–192.
25. Lowary,P.T. and Widom,J. (1998) New DNA sequence rules for high affinity binding to histone octamer and sequence-directed nucleosome positioning. *J. Mol. Biol.*, **276**, 19–42.
26. Dyer,P.N., Edayathumangalam,R.S., White,C.L., Bao,Y., Chakravarthy,S., Muthurajan,U.M. and Luger,K. (2004) Reconstitution of nucleosome core particles from recombinant histones and DNA. *Methods Enzymol.*, **375**, 23–44.
27. Eram,M.S., Kuznetsova,E., Li,F., Lima-Fernandes,E., Kennedy,S., Chau,I., Arrowsmith,C.H., Schapira,M. and Vedadi,M. (2015) Kinetic characterization of human histone H3 lysine 36 methyltransferases, ASH1L and SETD2. *Biochim. Biophys. Acta*, **1850**, 1842–1848.
28. Niu,L., Zhang,Y., Pei,Y., Liu,C. and Cao,X. (2008) Redundant requirement for a pair of PROTEIN ARGININE METHYLTRANSFERASE4 homologs for the proper regulation of Arabidopsis flowering time. *Plant Physiol.*, **148**, 490–503.
29. Schurter,B.T., Koh,S.S., Chen,D., Bunick,G.J., Harp,J.M., Hanson,B.L., Henschen-Edman,A., Mackay,D.R., Stallcup,M.R. and Aswad,D.W. (2001) Methylation of histone H3 by coactivator-associated arginine methyltransferase 1. *Biochemistry*, **40**, 5747–5756.
30. Mizoguchi,T., Hayashida,N., Yamaguchi-Shinozaki,K., Kamada,H. and Shinozaki,K. (1995) Two genes that encode ribosomal-protein S6 kinase homologs are induced by cold or salinity stress in Arabidopsis thaliana. *FEBS Lett.*, **358**, 199–204.
31. Fonseca,J.P., Steffen,P.A., Muller,S., Lu,J., Sawicka,A., Seiser,C. and Ringrose,L. (2012) In vivo Polycomb kinetics and mitotic chromatin binding distinguish stem cells from differentiated cells. *Genes Dev.*, **26**, 857–871.
32. Gehani,S.S., Agrawal-Singh,S., Dietrich,N., Christophersen,N.S., Helin,K. and Hansen,K. (2010) Polycomb group protein displacement and gene activation through MSK-dependent H3K27me3S28 phosphorylation. *Mol. Cell*, **39**, 886–900.
33. Lau,P.N. and Cheung,P. (2011) Histone code pathway involving H3 S28 phosphorylation and K27 acetylation activates transcription and antagonizes polycomb silencing. *Proc. Natl. Acad. Sci. U.S.A.*, **108**, 2801–2806.
34. Xu,L., Zhao,Z., Dong,A., Soubigou-Taconnat,L., Renou,J.P., Steinmetz,A. and Shen,W.H. (2008) Di- and tri- but not monomethylation on histone H3 lysine 36 marks active transcription of genes involved in flowering time regulation and other processes in Arabidopsis thaliana. *Mol. Cell. Biol.*, **28**, 1348–1360.
35. Kim,S.Y., He,Y., Jacob,Y., Noh,Y.S., Michaels,S. and Amasino,R. (2005) Establishment of the vernalization-responsive, winter-annual habit in Arabidopsis requires a putative histone H3 methyl transferase. *Plant Cell*, **17**, 3301–3310.
36. Zhao,Z., Yu,Y., Meyer,D., Wu,C. and Shen,W.H. (2005) Prevention of early flowering by expression of FLOWERING LOCUS C requires methylation of histone H3 K36. *Nat. Cell Biol.*, **7**, 1256–1260.
37. Keogh,M.C., Kurdistani,S.K., Morris,S.A., Ahn,S.H., Podolny,V., Collins,S.R., Schuldiner,M., Chin,K., Punna,T., Thompson,N.J. *et al.* (2005) Cotranscriptional set2 methylation of histone H3 lysine 36 recruits a repressive Rpd3 complex. *Cell*, **123**, 593–605.
38. Li,B., Gogol,M., Carey,M., Lee,D., Seidel,C. and Workman,J.L. (2007) Combined action of PHD and chromo domains directs the Rpd3S HDAC to transcribed chromatin. *Science*, **316**, 1050–1054.
39. Stroud,H., Hale,C.J., Feng,S., Caro,E., Jacob,Y., Michaels,S.D. and Jacobsen,S.E. (2012) DNA methyltransferases are required to induce heterochromatic re-replication in Arabidopsis. *PLoS Genet.*, **8**, e1002808.
40. Wysocka,J., Swigut,T., Xiao,H., Milne,T.A., Kwon,S.Y., Landry,J., Kauer,M., Tackett,A.J., Chait,B.T., Badenhorst,P. *et al.* (2006) A PHD finger of NURF couples histone H3 lysine 4 trimethylation with chromatin remodelling. *Nature*, **442**, 86–90.
41. Tsai,W.W., Wang,Z., Yiu,T.T., Akdemir,K.C., Xia,W., Winter,S., Tsai,C.Y., Shi,X., Schwarzer,D., Plunkett,W. *et al.* (2010) TRIM24 links a non-canonical histone signature to breast cancer. *Nature*, **468**, 927–932.
42. Chin,H.G., Patnaik,D., Esteve,P.O., Jacobsen,S.E. and Pradhan,S. (2006) Catalytic properties and kinetic mechanism of human recombinant Lys-9 histone H3 methyltransferase SUV39H1: participation of the chromodomain in enzymatic catalysis. *Biochemistry*, **45**, 3272–3284.
43. Zhang,X., Bernatavichute,Y.V., Cokus,S., Pellegrini,M. and Jacobsen,S.E. (2009) Genome-wide analysis of mono-, di- and trimethylation of histone H3 lysine 4 in Arabidopsis thaliana. *Genome Biol.*, **10**, R62.
44. Unni,S., Huang,Y., Hanson,R.M., Tobias,M., Krishnan,S., Li,W.W., Nielsen,J.E. and Baker,N.A. (2011) Web servers and services for electrostatics calculations with APBS and PDB2PQR. *J. Comput. Chem.*, **32**, 1488–1491.